REPORT DOCUMENTATION PAGE

Form Approved
OMB No. 0704-0188

1. REPORT DATE *(DD-MM-YYYY)*	**2. REPORT TYPE**	**3. DATES COVERED** *(From - To)*
01-05-2006	Conference Paper POSTPRINT	2005 - 2006

4. TITLE AND SUBTITLE
Manufacture and Experimental Analysis of a Concentrated Strain Based Deployable Truss Structure

5a. CONTRACT NUMBER

5b. GRANT NUMBER

5c. PROGRAM ELEMENT NUMBER

6. AUTHOR(S)
Juan M. Mejia-Ariza, Thomas W. Murphey*, Eric L. Pollard†

5d. PROJECT NUMBER

5e. TASK NUMBER

5f. WORK UNIT NUMBER

7. PERFORMING ORGANIZATION NAME(S) AND ADDRESS(ES) AND ADDRESS(ES)
Virginia Polytechnic Institute
& State University
2018 Hahn Hall
Blacksburg, VA 24061-0344

†CSA Engineering, Inc.
1600 Eubank Blvd SE
Albuquerque, NM 87123-3345

8. PERFORMING ORGANIZATION REPORT NUMBER

9. SPONSORING / MONITORING AGENCY NAME(S) AND ADDRESS(ES)
*Air Force Research Laboratory
Space Vehicles
3550 Aberdeen Ave SE
Kirtland AFB, NM 87117-5776

10. SPONSOR/MONITOR'S ACRONYM(S)

11. SPONSOR/MONITOR'S REPORT NUMBER(S)
AFRL-VS-PS-TP-2006-1029

12. DISTRIBUTION / AVAILABILITY STATEMENT
Approved for public release; distribution is unlimited. (Clearance #VS06-0152)

13. SUPPLEMENTARY NOTES
Published in the 47th AIAA/ASME/ASCE/AHS/ASC Structures, Structural Dynamics, and Materials Conference Proceedings, 1 – 4 May 2006, Newport, RI, AIAA 2006-1686

14. ABSTRACT
A truss structure was built and tested to advance deployable structures technology based on the concentrated strain approach. In 3rd order hierarchy systems, this architecture has the potential to provide a 10 fold improvement in mass efficiency, and demonstrate a linear compaction ratio that is five times better than current technology. A 101.6 cm x 12.7 cm x 12.7 cm test article was fabricated, and a buckling test and analysis was performed. The total mass of the deployable truss structure was 28 grams. This structure was constructed of piecewise constant cross section elements. One of the components consisted of high-modulus pull-truded carbon fiber rods (CFRs) for the majority of the length. The other components were compliant flexure joints made of Nitinol NiTi, a shape memory alloy (SMA) capable of a repeatable superelastic strain of 5.0% at either boundary. The results of this research provide a contribution to the deployable structures science by improving the compaction ratio and the mass efficiency of deployable structures without decreasing the truss performance limits.

15. SUBJECT TERMS
Deployable Stuctures; Concentrated Strain; Carbon Fiber Rods; CFRs; Shape Memory Alloy; SMA; Truss; Space Vehicles

16. SECURITY CLASSIFICATION OF:			**17. LIMITATION OF ABSTRACT**	**18. NUMBER OF PAGES**	**19a. NAME OF RESPONSIBLE PERSON**
a. REPORT	**b. ABSTRACT**	**c. THIS PAGE**			Thomas W. Murphey
Unclassified	Unclassified	Unclassified	Unlimited	11	**19b. TELEPHONE NUMBER** *(include area code)* 505-846-9969

47th AIAA/ASME/ASCE/AHS/ASC Structures, Structural Dynamics, and Materials Confere
1 - 4 May 2006, Newport, Rhode Island

AIAA 2006-1686

Manufacture and Experimental Analysis of a Concentrated Strain Based Deployable Truss Structure

Juan M Mejia-Ariza*
Virginia Polytechnic Institute and State University, Blacksburg, VA 24061-0344 US
Thomas W Murphey†
Air Force Research Laboratory, Albuquerque, NM 87117-5776 US
Eric L Pollard‡
CSA Engineering, Inc., Albuquerque, NM 87123-3345 US

A truss structure was built and tested to advance deployable structures technology based on the concentrated strain approach. In 3^{rd} order hierarchy systems, this architecture has the potential to provide a 10 fold improvement in mass efficiency, and demonstrate a linear compaction ratio that is five times better than current technology. A 101.6 cm x 12.7 cm x 12.7 cm test article was fabricated, and a buckling test and analysis was performed. The total mass of the deployable truss structure was 28 grams. This structure was constructed of piecewise constant cross section elements. One of the components consisted of high-modulus pull-truded carbon fiber rods (CFRs) for the majority of the length. The other components were compliant flexure joints made of Nitinol NiTi, a shape memory alloy (SMA) capable of a repeatable superelastic strain of 5.0% at either boundary. The results of this research provide a contribution to the deployable structures science by improving the compaction ratio and the mass efficiency of deployable structures without decreasing the truss performance limits.

Nomenclature

P_c	critical buckling force
I	moment of inertia
L	length
A_j	cross-sectional area of jth section
$(EI)_j$	flexural stiffness of jth section
l_1	length of outboard sections
l_2	half-length of center section
P	compressive load
F_c	buckling load
t	time
y_j	lateral displacement of jth section
x, ζ	longitudinal position coordinates
λ_{jk}	magnitude of kth root of characteristic polynomial for jth section
ψ_{jk}	kth root of characteristic polynomial for jth section
ω	vibration frequency

*Graduate Student, Macromolecular Science and Engineering Program, 2018 Hahn Hall, Blacksburg, VA 24061-0344 US.
†Engineer, Space Vehicles Directorate, 3550 Aberdeen Ave. SE, Albuquerque, NM 87117-5776 US, AIAA Professional Member.
‡Engineer, CSA Engineering, Inc., 1600 Eubank Blvd. SE, Albuquerque, NM 87123-3345 US, AIAA Young Professional Member.

I. Introduction

The research done in this paper is focused on the need to establish higher compaction ratio structures with greater mass efficiency. According to Murphey, it is possible to increase structural complexity that will lead to lighter weight structures. Murphey was able to establish that structural complexity enables lighter weight trusses subject to bending strength and stiffness requirements.[1,2] However, the approach in this paper is focused on concentrated strain approach, as a contrast to distributed strain systems as a means for compact packaging. According to Murphey, the components in deployable structures require a specific combination of high modulus for deployed strength and stiffness, and high strain limit for packaging and low density. In his research, a simple material performance index was derived for the mass efficiency of strain based deployable trusses. As a result ultra-high modulus carbon fibers with a typical strain of 0.2% are shown to score the highest performance index for traditional materials. Also, it was shown that optimal truss designs require only strains of less than 4% with high modulus materials.[2,3]

In Ref. 4, a high compaction ratio and extremely high mass efficient truss of trusses of solid rods was designed. This deployable structure is composed of ultra high modulus carbon fiber rods (P120 fiber), and Nickel-Titanium alloys with a superelastic response. These two elements are joined via unique fittings to allow the shape memory alloys to bend and consequently to release strain energy. The following flow chart summarizes the parameters design for the deployable truss; see Fig. 1.

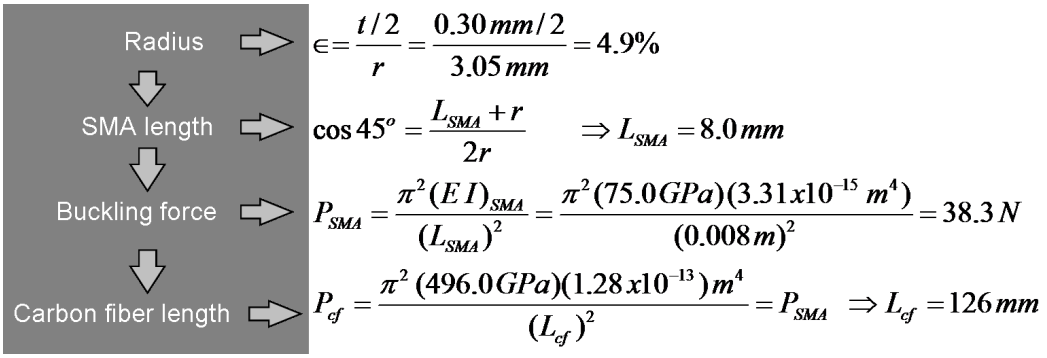

Figure 1. Flow chart for the parameters design of the deployable truss.

In the present work, carbon fiber rods (CFRs) and shape memory alloys (SMAs) will be assembled to create a structure that can be deployed through releasing of the strain energy stored in the SMAs. The tasks consist of structure fabrication and structure testing. The extruded CFR is made of continuous high-modulus carbon fibers in a vinyl-ester matrix. This material can be used as a higher structurally efficient material system for the majority of the element length because it is extremely stiff (modulus 136 GPa) and lightweight, and it has a very low thermal coefficient of expansion relative to the SMA(6.6 x $10^{-6}/^{\circ}C$ in martensite, 11 x $10^{-6}/^{\circ}C$ in austenite.[5] Unlike current deployable trusses, the carbon fiber rod segments of this system are optimized for one structural role, deployed configuration, as they are not required to articulate in order to package the structure. This allows higher modulus fibers to be used, like P120.

SMAs are materials that have the ability to return to a predetermined shape when heated. When this smart material is cold, or below its transformation temperature, it has a low yield strength that makes it easy to deform and retain its new shape. However, when this material is heated above its transformation temperature, it goes through an internal crystal structure change that allows it to recover its original shape. The most common SMA is an alloy of nickel and titanium called Nitinol.[6] This particular alloy has very good electrical and mechanical properties, long fatigue life, and high corrosion resistance. The corrosion resistance of NiTi alloys is highly sensitive to the surface conditions. It is highly dependent on the coupling material. Materials such as CFR, epoxy, and DSM Somos 11120 are safer to use as compared to precious metals such as Au and Pt that have strong galvanic effects.[5]

The SMA behavior considered in this paper is superelasticity. Superelasticity occurs when the material is deformed above the martensite start temperature, M_s, but still below the highest temperature at which it is possible to have martensite, M_d. There is an equivalence between temperature and stress: a decrease in temperature is equivalent to an increase in stress, both stabilizing martensite. Normally on cooling, the martensite forms at M_s under no stress. But in the same material, martensite can form above M_s if a stress

is applied, and the martensite so-formed is termed stress-induced martensite (SIM). The driving force for the transformation is now mechanical, as opposed to thermal. At a temperature above M_s but below M_d SIM is formed, leading to the usual superelastic loop with an upper and lower plateau.[7]

SMA is used in the truss as flexures because it is capable of repeatedly recovering from superelastic strains of 5.0%. This is an important characteristic as it allows for these features to replace typical mechanical joints found in similar deployable structures. Therefore, the SMAs are not only used to control the deployment process, but are also used as the hinges of the structure. This integrated dual role eliminates the need for secondary deployment actuators.

The fittings which interface the CFR and SMA segments are prototyped of DSM Somos 11120, a low viscosity liquid photopolymer that produces strong, tough, water resistant parts. Table 1 shows some typical properties of this material at ASTM D638M condition. Figure 2 illustrates the DSM Somos 11120 joint elements for the boom structure. There are two main kinds of joint element, type A and type B. When the truss is deploying the joint elements type A will have translation motion, but the joint elements type B will rotate. In a flight-like structure joint elements will be made of a more temperature and stress resistant material, like VECTRA that is of the family of the liquid crystalline polyesters (LCPs). LCPs are good for filling small parts that have high strength, are very stiff, and have high melting ($600°C$) properties.[8]

Hysol EA 9309.3 NA is used to bond the DSM Somos 11120 joint elements with the carbon fiber rods and the shape memory alloys.[9] This epoxy has high shear strength and good environmental resistance. This product requires mixing two components together just prior to application. The mix ratio by weight is 100 for part A (pink color) and 22 for part B (blue color). The amount of epoxy needed to bond the structure elements is very small, but the smallest amount that is found to be enough to work well is 5 grams of part A and 1.1 grams of part B. This adhesive may be cured for 3 to 5 days at 25 $°C$ or 1 hour at 82 $°C$ to achieve normal performance. However, the heat deflection temperature for the joint elements at 455 kPa is 46 - 54 $°C$, ASTM D648. Therefore, the selected cure temperature is set to be around 38 $°C$ for approximately twelve hours. Table 2 shows a typical tensile and compressive properties of Hysol EA 9309.3 NA at 25 $°C$. For the purposes of design, a good approximation for the temperature limits employed in aerospace systems is -50 $°C$ to +70 $°C$.[10] The material properties in this project do not have a considerable change for temperatures below +25 $°C$.

Table 1. Typical properties: DSM Somos 11120 post-cured part at ASTM D638M condition.

Measurement	Value
Tensile strength	47.0 - 53.6 MPa
Modulus of elasticity	2.67 - 2.88 GPa
Elongation at break	11 - 20%
Elongation at yield	3.3 - 3.5%

Table 2. Typical Tensile and Compressive Properties: Hysol EA 9309.3 NA

Measurement, 25 $°C$	Value
Tensile Modulus, ASTM D638	2.23 GPa
Compressive Modulus, ASTM D695	1.69 GPa

Figure 2. DSM Somos 11120 joint elements for the boom.

II. Manufacture

The side components of the boom have three different elements that need to be organized and classified before starting to assemble the structure. Nitinol with Ni 56.08% weight and Ti 43.02% weight is the SMA used to actuate the structure. This is a superelastic SMA that has a Young's modulus of approximately 75 GPa. The SMA is 0.030 cm x 0.147 cm, and its length changes depending on the joint element connection.

Table 3 and Table 4 present the quantity and length values of the SMAs and CFRs for their corresponding type of connection, respectively. The diameter of the carbon fiber rods is approximately 0.127 cm, and the corresponding length depends on the joint element connection at both ends of the rods. These dimensions are consistent with the structural system described in Ref. 4.

Table 3. Length and quantity base on the joint element connection for SMA.

Connection	Quantity	Length[cm]
B1	34	0.597
B2	34	0.596
B3	8	0.754
B4	8	0.922

Table 4. Length and quantity base on the joint element connection for CFR.

Connection	Quantity	Length[cm]
B1-B2	34	11.5
B1-B2	34	11.9
B1-B4	8	11.2
B2-B3	8	11.2

Three different fixtures are designed and built to construct the truss structure. The truss is composed of many similar kinds of side components. There are two kinds of side components: side component type A and side component type B. A picture of fixture 1, fixture 2 and fixture 3 is shown in Fig. 3, Fig. 4 and Fig. 7, respectively . Since the boom is a large and complex structure to manufacture, three copies of each fixture are constructed. These fixtures are considered the tools needed to fabricate the truss structure.

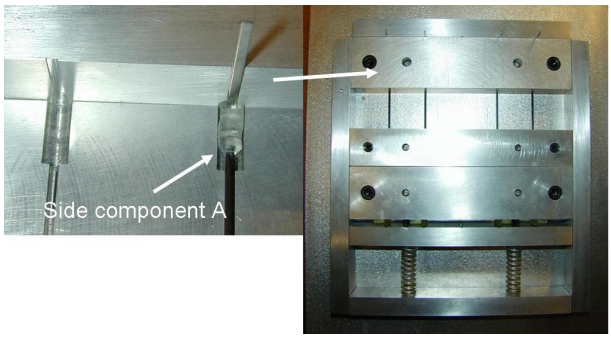

Figure 3. Fixture 1 connects the carbon fiber with the A type joints.

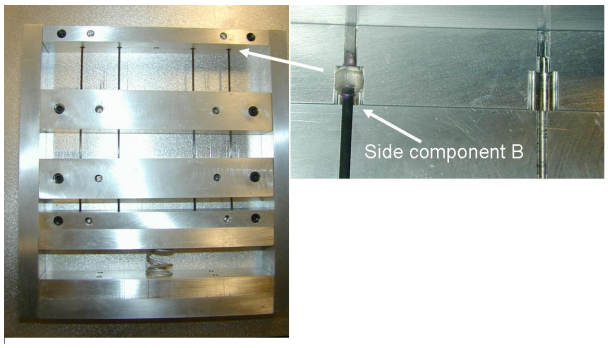

Figure 4. Fixture 2 connects the carbon fiber with the B type joints.

Fixture 1 is employed to connect the CFRs and the DSMs type A to assemble the corresponding side components type A as shown in Fig. 5. This fixture produces five side components type A at one time. Fixture 2 is used to join the CFRs, the DSM pieces type Bs, and the SMAs. This fixture produces five side components type B at once. Figure 6 presents the side component type B.

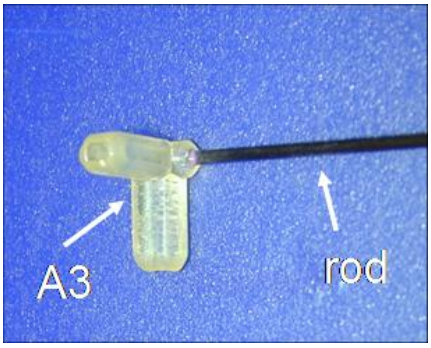

Figure 5. Side component type A made of joint element type A and carbon fiber rod.

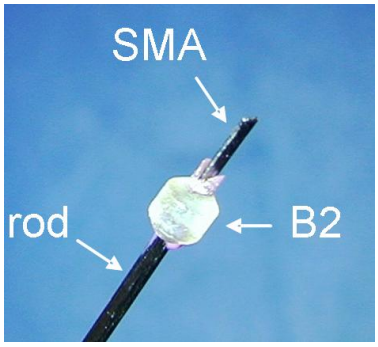

Figure 6. Side component type B made of joint element type B, CFR, and SMA.

Fixture 3 is utilized to attach side components type A and B to build four square faces at once. In addition, fixture 3 is used to connect two square faces to make a cubic box. Figure 7 illustrates a Hub box

made with fixture 3. Finally, fixture 3 can hook up two cubic boxes to create the truss structure. The truss structure consists of the truss body in the center and two hub boxes at the edges as shown in Fig. 8. The entire structure can be stowed into a very compact configuration. Additional truss bodies can be connected to the sides of the hub boxes in order to create a truss-of-trusses system.

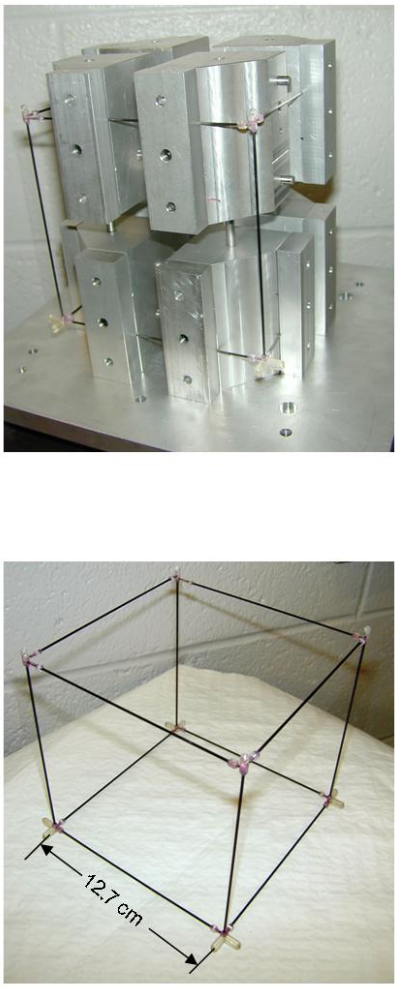

Figure 7. Fixture 3 connecting side components, and hub box made with fixture 3.

Figure 8. Deployable truss structure.

III. Experimental Analysis

A. Tension Test

Tension tests were performed to determine the modulus of the CFR and the SMA. Three specimens of each material were evaluated for some statistical significance. Figure 9 illustrates the tension test set up for the carbon fiber rod specimens. The strain is measured with a strain gage, and the stress is obtained with a load cell. The standard head displacement rate is 2 mm/min. Figure 10 shows the stress versus strain plots for one of the CFRs and one of the SMA samples. A linear curve fitting is done to obtain the slope that

represents the elastic modulus. The range of strain used to calculate the modulus for both materials is 0.001 - 0.003 cm/cm.[11]

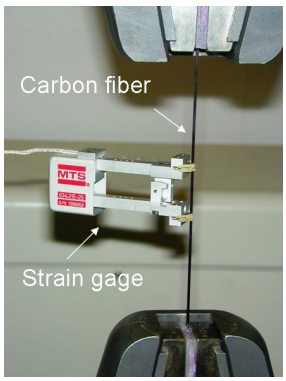

Figure 9. Tension test experimental set up for the CFR modulus.

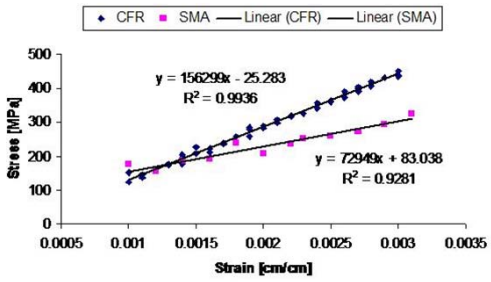

Figure 10. Stress versus strain and curve fitting of the CFR and the SMA.

Table 5 shows the experimental moduli of each material and the elastic modulus average value. The diameter of the CFR samples is 0.127 cm and their length is 13.8 cm, approximately. The dimensions of the SMA are 14.5 cm x .142 cm x 0.0279 cm. Both materials are clamped by 2.54 cm at each end.

B. Buckling Test for One Component

In order to test the performance of one single truss element, three elements were built with two joint elements with a CFR length of 11.2 cm and an SMA length of 1.11 cm. These two lengths have values traceable to the actual lengths found on the structure. The diameter of the CFR is 0.127 cm and the thickness and width of the SMA are $3.0510^{-2}cm$ and 0.147 cm respectively. The experimental buckling test set up is presented in Fig. 11. Figure 12 illustrates the experimental buckling test for one of the side component specimens. The experimental buckling force is 7.6 N and is calculated by obtaining the average value of the individual buckling forces of the three test articles. These buckling forces are 7.4 N, 7.6 N, and 7.8 N, and they occur at the point the load versus displacement trend no longer follows a linear trend. The initial slope in Fig. 12 is the compressive stiffness of the component. The experimental compresive stiffness is 46.6 N/mm and is calculated by obtaining the average value of the individual initial slopes of the three test articles. The compressive stiffnesses are 44.5 N/mm, 48.8 N/mm, and 46.4 N/mm.

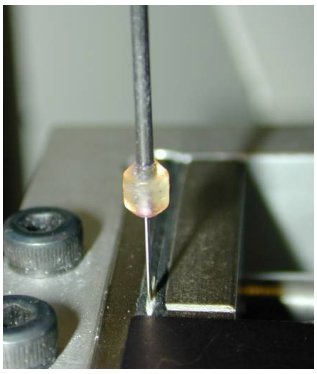

Figure 11. Experimental buckling test set up.

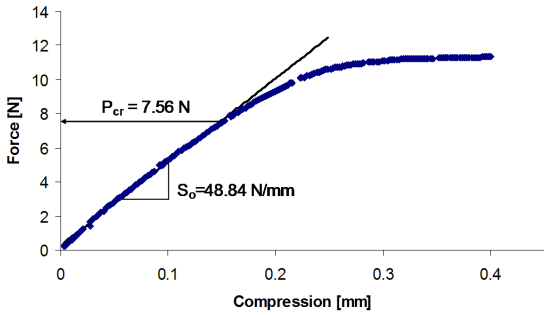

Figure 12. Experimental buckling load of a truss element.

IV. Numerical Analysis

A. Buckling Force for One Component

The buckling force of one truss component is determinated from a numerical solution of the exact eigenvalue problem, as shown in the Appendix. Lake's paper is selected in order to follow the same theoretical approach, but this time for a fixed-fixed supported column with a piecewise constant cross section.[12] This type of column configuration is the one that represents a single element in the deployable truss structure. For the derivations of the governing equations, only one-half of the column is considered for analysis as shown in Fig. 13. Assuming harmonic motion, the separation of variables method is applied to get the eigenvalues and eigenvectors. The critical buckling force is obtained when the static case is applied (natural frequency equal to zero). Using the parameter values in Table 6, the corresponding value of the critical buckling load is computed, 12.7 N, higher than the average experimental value, 7.6 N. In addition, for the same model the critical load value, 10.7 N, was computed with ABAQUS in Ref. 4 using finite element analysis (FEA). This value is still higher than the experimental value.

Table 5. Average moduli for the CFRs and SMAs.

sample	CFR modulus	SMA modulus
1	156.3	73.0
2	157.2	72.5
3	154.6	69.1
Average	156.0 GPa	71.5 GPa

Table 6. Parameters used for the buckling force analytical solution.

Parameter	SMA	CFR
Modulus (GPa)	71.5	156
Length (cm)	1.11	11.2
I (m^4)	0.34810^{-14}	0.12810^{-12}

B. Fixed-fixed column versus single support column

A simply supported column of uniform cross section is compared with a fixed-fixed support beam of piecewise constant cross section as shown in Fig. 14. The following equation is used to determine the critical load of the single support beam:

$$\mathrm{F_c} = \frac{\pi^2 E_2 I_2}{2L_2 + 2L_1}$$

where

$$L = 2L_2 + 2L_1, \quad E = E_2, and \quad I = I_2$$

The value obtained is 10.9 N smaller than the eigenvalue solution of the fixed-fixed support column buckling load, 12.7 N. However, it is almost the same as the FEA solution of the fixed-fixed support column buckling load, 10.7 N, in Ref. 4. This means that the new proposed model will a have higher compaction ratio with greater mass efficiency than a traditional deployable structure without decreasing the critical buckling force.

V. Conclusion

There are several contributions in this paper for the deployable structure science area. The principal idea is to be able to make a large deployable truss with a higher compaction ratio and greater mass efficiency than traditional deployable structures. The truss elaborated in this research was design to have in account these two improve parameters to make the deploy process more feasible. In order to meet these two parameters, it is expected to have a more refined design of the deployable truss. However, it was demonstrated in this work that it is possible to build a more geometric compound and large deployable structure with a simple set of fixtures. Therefore, a simple set of fixtures was designed and manufactured for the deployable truss. The materials and the component mechanisms used for the truss are simple and easy to implement. For example, five components made of carbon fiber rods and shape memory alloys are prepared at the same time with one fixture. An important characteristic of this fixture is that it keeps the two SMAs aligned at both ends of the carbon fiber rod when curing the epoxy. There is another fixture that joins the components in order to build squares and cubes. This fixture can also connect cubes of different sizes.

Tension tests were done to determinate the modulus of the carbon fiber rod and shape memory alloy. The average modulus values are 156 GPa and 71.5 GPa for CFR and SMA, respectively. However, the original

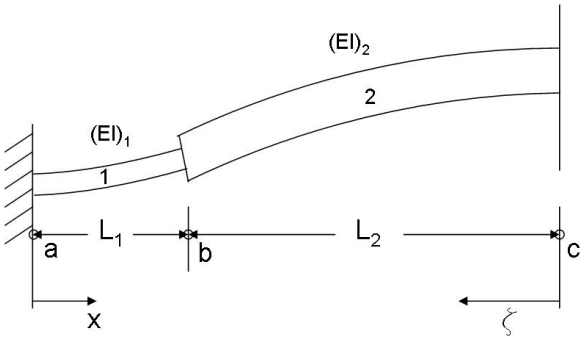

Figure 13. Analytical model

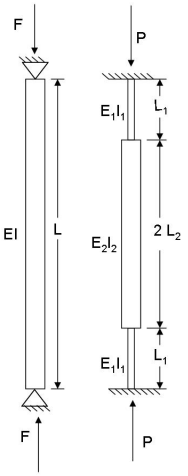

Figure 14. Schematic model for a single supported and fixed-fixed beam.

parameter design calculations are based on a P120 fiber with an estimated modulus value of 496.0 GPa. The final flight-like structure will be made of P120 because it has a high modulus value, making the structure stiffer. In addition, buckling tests were done and a critical buckling load of 7.6 N is obtained by calculating the average value of individual buckling forces for three side components. The numerical solution of the critical buckling load of a side component is determined by solving an exact eigenvalue problem. The critical buckling force obtained was 12.7 N, and it is higher than the experimental value, as well as the finite element solution in Ref. 4, 10.7 N. These two solutions are compared with the solution of a simple supported column with uniform cross section, 10.9 N. To be conservative the critical buckling load of the FEA solution was selected because it has a lower value than the eigenvalue solution. Since the buckling force value of the FEA solution is almost the same as the value of a simply supported column, the deployable truss in this research will have higher compaction ratio with greater mass efficiency than traditional deployable structures without decreasing the critical buckling force.

Appendix

1. Derivation of the Governing Equations

Because of the symmetry in geometry and loading, it is possible to consider only one-half of the column for analysis. The governing differential equations in section 1 and 2 are

$$\frac{\partial^4 y_1(x,t)}{\partial x^4} + \frac{P}{(EI)_1}\frac{\partial^2 y_1(x,t)}{\partial x^2} + \frac{\rho_1 A_1}{(EI)_1}\frac{\partial^2 y_1(x,t)}{\partial t^2} = 0$$

$$\frac{\partial^4 y_2(\zeta,t)}{\partial \zeta^4} + \frac{P}{(EI)_2}\frac{\partial^2 y_2(\zeta,t)}{\partial \zeta^2} + \frac{\rho_2 A_2}{(EI)_2}\frac{\partial^2 y_2(\zeta,t)}{\partial t^2} = 0 \tag{1}$$

Boundary Conditions:

$$y_1(x,t)|_{x=0} = \left.\frac{\partial y_1(x,t)}{\partial x}\right|_{x=0} = 0$$

$$\left.\frac{\partial y_2(\zeta,t)}{\partial \zeta}\right|_{\zeta=0} = \left.\frac{\partial^3 y_2(\zeta,t)}{\partial \zeta^3}\right|_{\zeta=0} = 0 \tag{2}$$

Displacement

$$y_1(x,t)|_{x=l_1} = y_2(\zeta,t)|_{\zeta=l_2} \tag{3}$$

Slope of the deflection

$$\left.\frac{\partial y_1(x,t)}{\partial x}\right|_{x=l_1} = -\left.\frac{\partial y_2(\zeta,t)}{\partial \zeta}\right|_{\zeta=l_2} \tag{4}$$

Bending moment

$$(EI)_1 \frac{\partial^2 y_1(x,t)}{\partial x^2}\bigg|_{x=l_1} = (EI)_2 \frac{\partial^2 y_2(\zeta,t)}{\partial \zeta^2}\bigg|_{\zeta=l_2} \tag{5}$$

Shearing force

$$(EI)_1 \frac{\partial^3 y_1(x,t)}{\partial x^3}\bigg|_{x=l_1} = -(EI)_2 \frac{\partial^3 y_2(\zeta,t)}{\partial \zeta^3}\bigg|_{\zeta=l_2} \tag{6}$$

Notice that the minus signs exist because the x and ζ coordinates axes are in opposite directions.

Assuming harmonic motion and applying separation of variables gives the following forms for the lateral displacements:

$$\begin{aligned} y_1(x,t) &= ce^{i\omega t}e^{\psi_1 x} \\ y_2(\zeta,t) &= ce^{i\omega t}e^{\psi_2 \zeta} \end{aligned} \tag{7}$$

Characteristic polynomials in ψ_1 and ψ_2:
Section 1:

$$\psi_1^4 + \frac{P}{(EI)_1}\psi_1^2 + \frac{\rho_1 A_1}{(EI)_1}\omega^2 = 0$$

so that

$$\psi_{11} = \pm i\sqrt{\frac{P + (P^2 + 4\rho_1 A_1 (EI)_1 \omega^2)^{1/2}}{2(EI)_1}}$$

and

$$\psi_{12} = \pm\sqrt{\frac{-P + (P^2 + 4\rho_1 A_1 (EI)_1 \omega^2)^{1/2}}{2(EI)_1}} \tag{8}$$

Section 2:

$$\psi_2^4 + \frac{P}{(EI)_2}\psi_2^2 + \frac{\rho_2 A_2}{(EI)_2}\omega^2 = 0$$

so that

$$\psi_{21} = \pm i\sqrt{\frac{P + (P^2 + 4\rho_2 A_2 (EI)_2 \omega^2)^{1/2}}{2(EI)_2}}$$

and

$$\psi_{22} = \pm\sqrt{\frac{-P + (P^2 + 4\rho_2 A_2 (EI)_2 \omega^2)^{1/2}}{2(EI)_2}} \tag{9}$$

2. Solutions for Column Buckling

The equations of the previous section can be solved to determine the critical buckling load of the column by assuming the vibration frequency to be zero. For $\omega = 0$, $\psi_{12} = \psi_{22} = 0$ and the general solution can be written as follows for the two sections of the column.

$$\begin{aligned} Y_1(x) &= C_{11}\sin(\lambda_{11}x) + C_{12}\cos(\lambda_{11}x) + C_{13}x + C_{14} \qquad (0 \le x \le l_1) \\ Y_2(\zeta) &= C_{21}\sin(\lambda_{21}\zeta) + C_{22}\cos(\lambda_{21}\zeta) + C_{23}\zeta + C_{24} \qquad (0 \le \zeta \le l_2) \end{aligned} \tag{10}$$

where $C_{11}, C_{12}, C_{13}, C_{14}, C_{21}, C_{22}, C_{23}$ and C_{24} are arbitrary constants and λ_{11} and λ_{21} are the magnitudes of the roots of the characteristic polynomial ψ_{11} and ψ_{21} given, respectively by

$$\lambda_{11} = \sqrt{\frac{P_c}{(EI)_1}} \quad and \quad \lambda_{21} = \sqrt{\frac{P_c}{(EI)_2}} \tag{11}$$

Application of the boundary conditions gives the following system of equations for C_{11}, C_{12}, C_{22} and C_{24}:

$$\begin{bmatrix} \sin(\lambda_{11}l_1) - \lambda_{11}l_1 & \cos(\lambda_{11}l_1) - 1 & -\cos(\lambda_{21}l_2) & -1 \\ \lambda_{11}\cos(\lambda_{11}l_1) - \lambda_{11} & -\lambda_{11}\sin(\lambda_{11}l_1) & -\lambda_{21}\sin(\lambda_{21}l_2) & 0 \\ -(EI)_1\lambda_{11}^2\sin(\lambda_{11}l_1) & -(EI)_1\lambda_{11}^2\cos(\lambda_{11}l_1) & (EI)_2\lambda_{21}^2\cos(\lambda_{21}l_2) & 0 \\ -(EI)_1\lambda_{11}^3\cos(\lambda_{11}l_1) & (EI)_1\lambda_{11}^3\sin(\lambda_{11}l_1) & (EI)_2\lambda_{21}^3\sin(\lambda_{21}l_2) & 0 \end{bmatrix} \begin{pmatrix} C_{11} \\ C_{12} \\ C_{22} \\ C_{24} \end{pmatrix} = \begin{pmatrix} 0 \\ 0 \\ 0 \\ 0 \end{pmatrix} \quad (12)$$

The existence of a nontrivial solution of the previous equation requires that

$$\begin{aligned} &(EI)_2\lambda_{21}^2\cos(\lambda_{11}l_1)\sin(\lambda_{21}l_2) + (EI)_2\lambda_{11}\lambda_{21}\cos(\lambda_{21}l_2)\sin(\lambda_{11}l_1) \\ &-(EI)_2\lambda_{21}^2\sin(\lambda_{21}l_2) + (EI)_1\lambda_{11}^2\sin(\lambda_{21}l_2) = 0 \end{aligned} \quad (13)$$

Substituting the definitions for λ_{11} and λ_{21}, Eq. 11, in the transcendental equation, Eq. 13, and plotting the left side of Eq. 13, the buckling load, $P_c = 12.7N$, is the first axial intersect, as shown in Fig. 15.

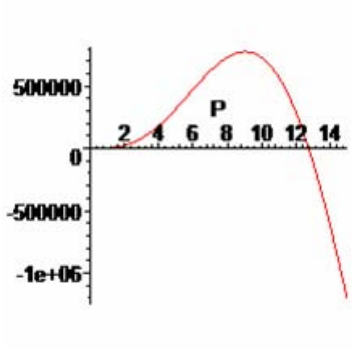

Figure 15. Plot of the transcendental equation.

Acknowledgements

This work was supported by the Air Force Research Laboratory, Space Vehicles Directorate. Dr. Jeffry Welsh is the program chief. The authors gratefully acknowledge the support.

References

[1]Murphey, T. W., and Hinkle, J. D., Some Performance Trends in Hierarchical Truss Structures, 44th AIAA Structures, Structural Dynamics, and Materials Conference, AIAA Paper 2003-1903, April 2003.

[2]Murphey, T. W., *Booms and Trusses*, Space Vehicles Directorate, U.S. Air Force Research Laboratory, Kirtland Air Force Base, New Mexico, P. 1-43.

[3]Murphey, T. W., A Material Structural Performance Index for Strain Based Deployable Trusses, 45th AIAA Structures, Structural Dynamics, and Materials Conference, AIAA Paper 2004-1569, April 2004.

[4]Pollard, E., "Development of a Concentrated Strain Based Deployable Truss Structure," 47th AIAA, Structural Dynamics and Materials Conference (to be published).

[5]Memry Corporate, Headquarters and Eastern Operations, Nitinol FAQ, URL: http://www.memry.com/nitinolfaq/nitinolfaq.html, [cited 1 April 2006].

[6]MatWeb.com, The Online Materials Database, Nitinol-NiTi Shape Memory Alloy; High-Temperature Phase, URL: http://www.matweb.com/search/SpecificMaterial.asp?bassnum=MTiNi0/, [cited 1 April 2006].

[7]Wayman, C. M., and Duerig, T. W., *An Introduction to Martensite and Shape Memory*, Butterworth-Heinemann, Engineering Aspects of Shape Memory Alloys (UK), 1990, P. 3-20.

[8]Jackson, W. J., and Kuhfuss, H. F., "Liquid Crystalline Polyesters," Journal of Polymer Science, Part A: Polymer Chemistry, Vol. 14, No. 2043, 1976.

[9]Henkel Corporation, Aerospace Group, URL: http://www.aerospace.henkel.com/, [cited 1 April 2006].

[10]Schetky, L. M., "Shape memory alloy applications in space systems," Materials and Design Journal, Vol. 12, No. 1, 1991.

[11]ASTM 2D3039/D3039M-00e2, *Standard Test Method for Tensile Properties of Polymer Matrix Composite Materials*, copyright 2005 ASTM International Standards.

[12]Lake, M. S., and Mikulas, M. M., "Buckling and Vibration Analysis of a Simply Supported Column with a Piecewise Constant Cross Section," NASA TP-3090, 1991.